ADVANCED FUNCTIONAL MATERIALS
www.afm-journal.de

www.MaterialsViews.com

Dual-Salt Mg-Based Batteries with Conversion Cathodes

*Ye Zhang, Junjie Xie, Yanlin Han, and Chilin Li**

Mg batteries as the most typical multivalent batteries are attracting increasing attention because of resource abundance, high volumetric energy density, and smooth plating/stripping of Mg anodes. However, current limitations for the progress of Mg batteries come from the lack of high voltage electrolytes and fast Mg-insertable structure prototypes. In order to improve their energy or power density, hybrid systems combining Li-driven cathode reaction with Mg anode process appear to be a potential solution by bypassing the aforementioned limitations. Here, FeS_x (x = 1 or 2) is employed as conversion cathode with 2–4 electron transfers to achieve a maximum energy density close to 400 Wh kg^{-1}, which is comparable with that of Li-ion batteries but without serious dendrite growth and polysulphide dissolution. In situ formation of solid electrolyte interfaces on both sulfide and Mg electrodes is likely responsible for long-life cycling and suppression of S-species passivation at Mg anodes. Without any decoration on the cathode, electrolyte additive, or anode protection, a reversible capacity of more than 200 mAh g^{-1} is still preserved for Mg/FeS_2 after 200 cycles.

1. Introduction

Due to high safety and cost cutting, rechargeable multivalent batteries (e.g., Mg, Al, and Ca ones) are becoming a new focus as an alternative technology beyond Li-ion batteries (LIBs).[1,2] Compared with Li metal, Mg metal has a much higher volumetric capacity of 3833 mAh cm^{-3} (vs 2205 mAh cm^{-3} for Li), and its reduction potential (–2.4 V vs standard hydrogen electrode) is only 0.6 V higher.[1] These would not result in a serious compromise of energy density of Mg-based batteries as long as coupled with suitable cathode materials. Furthermore, unlike Li metal with serious dendrite propagation problem, Mg metal as anode is thought to be dendrite-free during electrochemical deposition/dissolution.[1] Although Mg^{2+} (0.86 Å) has a similar ionic radius as that of Li^+ (0.9 Å), its high charge density and polarity usually lead to a low solid-diffusion rate of Mg^{2+} in most of the crystal structures.[3] An exception is the Chevrel phase (e.g. Mo_6S_8), where octahedral Mo_6 clusters enable a fast and efficient achievement of local electroneutrality upon Mg^{2+} insertion.[3] However, its energy density is very limited in view of a theoretical capacity of 122 mAh g^{-1} (corresponding to two Mg^{2+} insertion into one Mo_6S_8 host) and a moderate voltage (1.1–1.2 V vs Mg^{2+}/Mg).

In order to extend the choice of cathode and circumvent the sluggish Mg^{2+} transport in host lattices, recently a concept of dual-salt polyvalent metal storage was proposed, where e.g., Li^+ instead of Mg^{2+} is inserted into cathode from the Li-ion reservoir of dual-salt electrolyte during discharge and at metallic Mg anode Mg^{2+} is preferentially electrodeposited over Li^+ during charge.[4] It indicates that many Li-insertable materials can become the candidates of cathode as long as their reaction voltages do not exceed the electrochemical window of present Mg-based electrolyte systems. Furthermore Li-dendrite problem appears to be avoidable in this hybrid Mg/Li battery (MLB) design. Some sulfides and oxides (e.g., TiS_2, TiO_2, and $Li_4Ti_5O_{12}$) have been attempted as cathodes in view of their moderate voltages (<1.5 V) matching well with two typical dual-salt electrolytes, i.e., all-phenyl complex (APC) coupled with lithium chloride (LiCl) and magnesium borohydride ($Mg(BH_4)_2$) with lithium borohydride ($LiBH_4$).[5–10] Their good rate and cycling performances benefit from faster Li^+ insertion at cathode and safer Mg^{2+} deposition at anode. So far, resorting to higher voltage Li-ion cathodes (e.g., $LiFePO_4$) seems to be unsuccessful due to quick electrolyte degradation.[4] Therefore, in this work, we propose to utilize Li-driven conversion reaction instead of insertion one in order to significantly improve the capacity performance of Mg-based batteries for the first time.

Here, two typical resource-abundant sulfides FeS_2 and FeS are investigated as compatible conversion electrodes in Mg-based batteries. Although FeS_2 has been assigned as primary and secondary Li battery cathodes for many years, its advantage of high capacity (a theoretical value of 894 mAh g^{-1} referring to four electron transfer based on Fe^{2+}/Fe^0 and S_2^{2-}/S^{2-}) is seriously counteracted by the dissolution of polysulfide intermediate products as well as Li-dendrite growth, which cause a quick capacity fading during cycling as in Li/S systems.[11,12] Therefore, the similar strategies for Li/S batteries can be copied to Li/FeS_2 ones, including cathode coating (e.g., by PAN), utilization of polysulfide-dissolution repressible electrolytes

Y. Zhang, Dr. J. Xie, Y. Han, Prof. C. Li
State Key Laboratory of High Performance Ceramics and Superfine Microstructure
Shanghai Institute of Ceramics
Chinese Academy of Sciences
Shanghai 200050, P. R. China
E-mail: chilinli@mail.sic.ac.cn
Y. Zhang
University of Chinese Academy of Sciences
Beijing 100039, P. R. China
Y. Han
College of Environmental and Chemical Engineering
Shanghai University
Shanghai 200444, P. R. China

DOI: 10.1002/adfm.201503639

(e.g., ionic liquid), or all solid-state architectures (e.g., sulfide-based Li-ion conductor as solid electrolyte).[13–15] Li-driven conversion of FeS (with a theoretical value of 609 mAh g^{-1} referring to two electron transfer based on Fe^{2+}/Fe^0) is less complex than FeS_2 owing to the absence of anionic redox process, and is expected to possess better reversibility in common nonaqueous electrolytes.[16] Compared with the innovations on cathode and electrolyte in the past years, the anode treatment for sulfur- or sulfide-based batteries is rarely explored apart from electrolyte additive (e.g., $LiNO_3$) and hybrid anode design (e.g., lithiated graphite on metallic Li).[17,18] Although these strategies enable the formation of artificial solid electrolyte interface (SEI) layer at anode and the suppression of shuttle effect, a gradual corrosion of Li metal is still inevitable as a consequence of electrolyte consumption and SEI porosity.[19]

In this work, we displace metallic Li by Mg at anode and meanwhile employ dual-salt electrolytes with adjustable concentration of Mg^{2+} and Li^+. This hybrid MLB design allows a combination of highly reversible Li-driven conversion processes and Mg plating/stripping without any cathode decoration and electrolyte additive. It bypasses the slow Mg^{2+} diffusion in host lattices and unsafe Li-dendrite propagation. Unlike previous MLB systems characterized by structure integrity and single electron transfer at cathode,[4–10] in our case multielectron transfers are simultaneously satisfied at both the electrodes. Depending on the concentration of Li salts in hybrid electrolytes, Mg/FeS_2 and Mg/FeS batteries achieve a maximum reversible capacity of 600 and 520 mAh g^{-1} at 0.05 C respectively. Better reversibility (surviving up to hundreds of cycles) than Li/FeS_x is associated with in situ formation of SEI with unique components on both the sulfide and Mg surfaces, which effectively mitigate polysulfide dissolution, shuttle phenomenon, and anode passivation.

2. Results

2.1. Electrochemistry of Mg/FeS_x Batteries Depending on Electrolyte Type, Li-Salt Concentration, and Cutoff Voltage

Figures S1 and S2 (Supporting Information), respectively, show the scanning electron microscope (SEM) images and X-ray diffraction (XRD) patterns of the commercially available FeS_2 and FeS samples. Their microsized monolithic or aggregate morphologies are in favor of the improvement on volumetric energy density. Most of the primary FeS_2 particles have a size of 100–200 nm apart from few larger polyhedral grains (Figure S1a,b, Supporting Information). They aggregate to form much larger secondary granules with several micrometers in dimension and sufficient porosity. The primary particles of FeS (≈50 nm in size) are smaller than those of FeS_2; however, they are more compactly adhered with each other leading to the formation of microsized monolith with less voids (Figure S1c,d, Supporting Information). FeS_2 sample mainly consists of cubic pyrite phase (p-FeS_2) with minor marcasite impurity (m-FeS_2), whereas FeS sample is mainly composed of two different hexagonal phases (Figure S2, Supporting Information).

Figure 1a,b, respectively, presents the galvanostatic curves of FeS_2 and FeS (vs Mg metal) performed in a hybrid electrolyte with 0.1 M $Mg(BH_4)_2$ and 1.5 M $LiBH_4$ with a voltage range of 0.1–1.7 V and a current density of 0.05 C. Their initial discharge capacities of 845 mAh g^{-1} (95% of the theoretical value of FeS_2) and 587 mAh g^{-1} (97% of the theoretical value of FeS) are achieved mainly by a plateau behavior at 0.7 and 0.5 V, respectively. Their reversible discharge capacities are preserved at 600 and 520 mAh g^{-1} respectively with a substantial plateau around 0.7 V for both the samples. Their energy densities (i.e., 396.2 Wh kg^{-1} for FeS_2 and 320.3 Wh kg^{-1} for FeS) are much larger than those of previously reported MLB systems based on insertion cathodes (e.g., ≈160 Wh kg^{-1} for Mo_6S_8 or ≈290 Wh kg^{-1} for TiS_2) under the comparable rate and Li-salt concentration,[5–10] indicating the advantage of conversion reaction on capacity release without serious tradeoff of reaction voltage. For Mg/FeS_2 the following discharge processes show a voltage-similar plateau as the first discharge but with a capacity shrinkage of 30%. Therein about one-fourth capacity (150 mAh g^{-1}) is contributed from a higher voltage region from 1.3 to 0.75 V, which is not found during the first discharge, indicating an irreversible phase transformation during the 1st cycle. The similar phenomena also occur in Li/FeS_2.[11] In contrast, an upward shift of plateau voltage by 0.2 V (from 0.5 to 0.7 V) is observed for Mg/FeS. It is likely associated with the electrochemical amorphization or pulverization of FeS as discussed later. Owing to a simpler phase transformation process without the participation of disruption/recombination of $(S–S)^{2-}$ bond, FeS displays better capacity preservation than FeS_2 with an initial capacity loss of merely 8.5%. The first and following charge profiles are similar with a substantial plateau around 1 V for both the sulfides. This borohydride-based electrolyte does not bring about remarkable shuttle phenomenon associated with the dissolution of polysulfide species. A trace of charge capacity near 1.7 V should be caused by electrolyte instability and/or the possible oxidation to longer chain S_n^{2-} ($n \geq 4$) anions.[20,21] We also attempted another dual-salt chloride-based electrolyte containing 0.25 M APC and 1.0 M LiCl with the same upper cutoff voltage of 1.7 V (Figure 1c). Taking FeS_2 as the example, both the rate and reversibility performances are inferior to those in borohydride-based electrolyte. Its first discharge capacity at 0.1 C is 675 mAh g^{-1} (vs 725 mAh g^{-1} for borohydride-based electrolyte as shown in Figure 1d), whereas its reversible capacity degrades from 425 to 340 mAh g^{-1} during 2nd–6th cycles (where that is preserved at ≈500 mAh g^{-1} for borohydride-based electrolyte). APC solution is thought to be more vulnerable to polysulfide dissolution than diglyme solvent in borohydride-based electrolyte. As magnesium organohaloaluminate electrolytes are nucleophilic and incompatible with an electrophilic sulfur or polysulfide cathode,[22] the APC solution consisting of PhMgCl is easy to be attacked by polysulfide anions or radials. It should be one of the main reasons for worse FeS_2 electrochemistry in APC-based electrolyte.

Note that the electrochemical activity of Mg/FeS_2 greatly depends on Li-salt concentration and upper cutoff voltage. Its reversible capacity at 0.1 C decreases to 370 and 190 mAh g^{-1} with the corresponding dilution of $LiBH_4$ to 1 and 0.5 M (Figure 1d). When no Li-salt is added (i.e., 0 M $LiBH_4$), the capacity is almost negligible (Figure S3, Supporting Information), indicating a poor plating/stripping kinetics of Mg anode due to insufficiency of coordination ligand BH_4^- or negligible

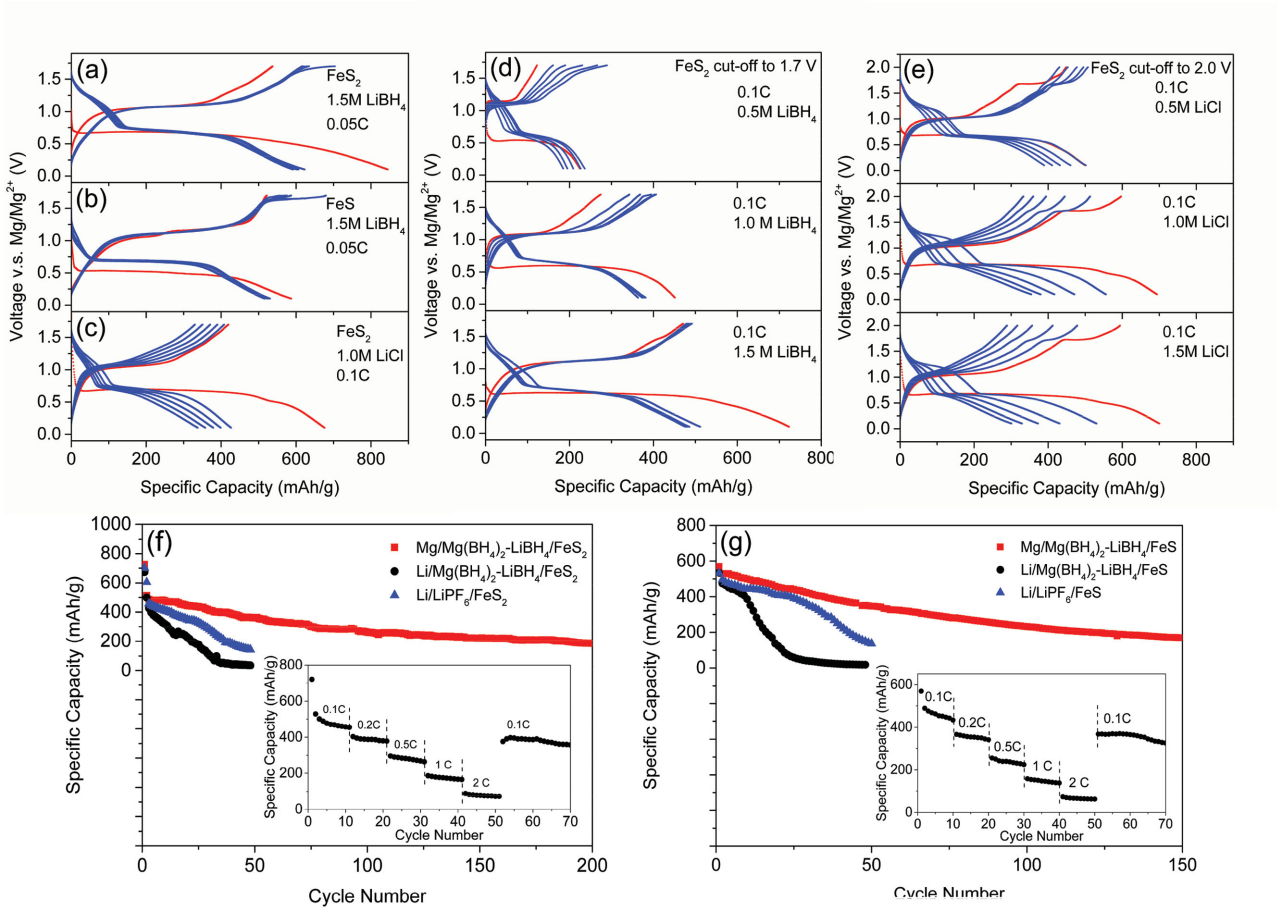

Figure 1. Galvanostatic charge–discharge curves of a) FeS_2 and b) FeS as conversion cathodes by using a borohydride-based electrolyte with 1.5 M $LiBH_4$ during the first six cycles at 0.05 C and c) of FeS_2 by using a chloride-based electrolyte with 1.0 M LiCl at 0.1 C. Galvanostatic charge–discharge curves of FeS_2 electrodes by using d) a borohydride-based and e) a chloride-based electrolytes with different Li-salt concentrations (from 0.5 to 1.5 M) and upper cut-off voltages (to 1.7 or 2.0 V) at 0.1 C. Discharge capacities of f) Mg/FeS_2 and g) Mg/FeS batteries as a function of cycling number at 0.1 C by using a borohydride-based electrolyte with 1.5 M $LiBH_4$. The cycling stability of discharge capacities of Li/$Mg(BH_4)_2$–$LiBH_4$/FeS_x and Li/$LiPF_6$/FeS_x batteries is also plotted as a comparison. Insets of (f) and (g): Corresponding rate performance of Mg/FeS_x batteries from 0.1 C to 2 C. The Mg anode and borohydride-based electrolyte render the batteries better capacity retention. The remarkable dependence of the capacity on the Li-salt concentration of hybrid electrolytes indicates a Li-driven conversion reaction process at the cathode.

Mg^{2+} insertion capability at cathode.[20,23] Consistently, both the charge/discharge polarization and coulombic efficiency (CE) become worse with less Li-salt addition (Table S1, Supporting Information). The initial discharge capacity of Mg/FeS_2 with lower $LiBH_4$ concentration is far away from its theoretical value, indicating a substantial residual of unreacted FeS_2, which gradually participates the conversion reactions during the following cycles therein with increasing capacities close to or even exceeding the initial one (Figure 1d). Chloride-based electrolyte is thought to have wider electrochemical window than borohydride-based one;[5,7,8] therefore, we extend the upper cutoff voltage to 2 V in chloride-based system to allow the appearance of a new charge plateau above 1.7 V (Figure 1e). Correspondingly, the following discharge at higher-voltage region (0.75–1.3 V) releases a larger capacity (e.g., 230 mAh g^{-1}, one-third of the total capacity for 1 M LiCl) than under a lower cutoff voltage of 1.7 V. However, such a capacity gain is quickly counteracted by the degradation of electrochemical curves mainly referring to two sets of redox plateaus as also observed in Li/FeS_2 (Figure S4, Supporting Information), where the dissolution of long-chain polysulfide intermediates is thought to be the main reason for degradation.[11] Both the polarization and CE dependences on LiCl concentration seem to show the opposed tendencies to $LiBH_4$ (Table S2, Supporting Information). In the case of 0.5 M LiCl, a relatively better preservation of redox plateaus is ascribed to incomplete initial conversion of FeS_2, which is continued during the later cycles. When LiCl concentration increases from 1 to 1.5 M, the first discharge capacity is not further activated, agreeing with weaker dissolution capability of LiCl than $LiBH_4$ in respective dual-salt electrolytes. A supersaturated electrolyte (e.g., 1.5 M LiCl) does not take effect on alleviating capacity degradation and on the contrary it accelerates this process as shown in Figure 1e. Similar to Li/FeS, the redox plateaus locating at higher voltage are not expected for Mg/FeS system in view of its one-step conversion process.[16]

As aforementioned, borohydride-based electrolyte renders Mg/FeS_x batteries better capacity retention than chloride-based one; meantime a cutoff voltage not exceeding 1.7 V is

expected to be favorable to suppress the formation of soluble polysulfides.[21] Therefore, we mainly concern about the cycling performance of Mg/FeS_x batteries using borohydride-based electrolyte with 1.5 M $LiBH_4$ and a cutoff voltage of 1.7 V as shown in Figure 1f,g. Their reversible capacities at 0.1 C lie between 350 and 400 mAh g^{-1} after 50 cycles, and are preserved at >200 mAh g^{-1} after 150–200 cycles. Under the rates as high as 0.5 C, 1 C, and 2 C, their discharge capacities are still maintained at ≈250, ≈150, and ≈50 mAh g^{-1} respectively for both the sulfides. Note that the involvement of anionic $(S–S)^{2-}$ redox process does not compromise the cyclability and rate performance of FeS_2 compared with simply converted FeS.

To further emphasize on the advantage of Mg anode over Li, Li/FeS_x batteries are investigated by using either the commonly used electrolyte (EC:DEC = 1:1) with 1 M $LiPF_6$ or the aforementioned dual-salt electrolyte with 1.5 M $LiBH_4$ (Figures S4 and S5, Supporting Information). For Li/FeS_2 in EC/DEC, two characteristic discharge plateaus at 2 and 1.5 V degrade quickly even when charging to 2.5 V (rather than 3V) in order to avoid the upper charge plateau referring to more soluble species. In borohydride-based systems with a cutoff voltage of 2.4 V, such an electrochemical degradation is still evident. In fact, few electrolytes can be applied in Li/FeS_2 due to corrosion of dissolved polysulfide toward Li metal, which would accelerate the further dissolution of polysulfide from cathode. Mg anode with potential SEI decoration is thought to be resistant to the corrosion of polysulfide and therefore enables the suppression of polysulfide dissolution as discussed later. Much better capacity retention and CE especially at higher rates when displacing Li by Mg in the same electrolyte confirm the advantage of safer and smoother Mg plating. As far as Li/FeS is concerned, a couple of well-defined redox plateaus is observed to be reversible around 1.7 V during the early cycles in EC/DEC or borohydride electrolytes (Figure 1g and Figure S5, Supporting Information). Although less dissolution of polysulfides in Li/FeS is responsible for better capacity retention than in Li/FeS_2, large volume change (up to 200%) and Li-dendrite growth still lead to a remarkable capacity fading in Li/FeS after 10–25 cycles.[16]

2.2. Conversion Reaction Mechanisms for Mg/FeS_x Batteries

So far, it is still unclear whether Li or Mg exclusively drives the conversion reaction, or Li and Mg codrive this process. Considering the similarity of electrochemical features of Mg/FeS_x to those of Li/FeS_x regardless of voltage levels, it is reasonable to believe that a substantial amount of Li should react with FeS_x at cathode. Figure S6a,b (Supporting Information) shows the ex situ XRD patterns of both the sulfides at different reaction stages by using borohydride-based electrolyte with 1.5 M $LiBH_4$. Both the diffraction peaks are significantly weakened with the deepening of discharge and almost no diffraction signals of products can be detected at the end of discharge to 0.1 V. Such an electrochemical amorphization is irreversible for both the sulfides (i.e., their recharged phases are still poorly crystallized). We resort to high-resolution transmission electron microscope (HRTEM) to further disclose the structure and distribution information of poorly crystallized products as shown in **Figure 2**. When discharging FeS_2 to 0.1 V, we found numerous nanoparticles (dark contrast) are generated and uniformly embedded in gel-like matrix (light contrast). Therein some nanoparticle aggregates of moderate size (100–200 nm) still exist (Figure 2a). The electrochemical pulverization progresses during the 2nd discharge, resulting in finer dispersed nanoparticles with a size as small as 5–10 nm (Figure 2b). The lattice fringes in these nanodomains are assigned to zero-valent Fe, agreeing with the selected area electron diffraction (SAED) patterns where the vague diffraction rings belong to Fe and Li_2S (Figure 2c). The discharged FeS shows the similar phase composition and distribution as FeS_2 according to its HRTEM and SAED (Figure S7a,b, Supporting Information). But its nanoparticles with a homogeneous size of about 50 nm are connected with each other to form porous aggregates, where the gel-like matrix appears to be absent. When FeS_2 is recharged to 1.7 V, the microstructure of nanoparticle-in-matrix is preserved with nanodomains mainly consisting of Fe_7S_8 and m-FeS_2 phases (Figure 2d,e). Few nanodomains belonging to Li_2FeS_2 and p-FeS_2 phases are also found occasionally (Figure 2f). This result confirms the statement by Lee and co-workers that nanocrystalline m-FeS_2 together with nonstoichiometric Fe_7S_8 can be electrochemically synthesized.[13–15] It also indicates that metastable Li_2FeS_2 intermediate can stably exist.[11] The reappearance of stoichiometric FeS_2 after recharge benefits from less dissolution of S-based species. For FeS, recharge process does not bring about recovering of crystallization (Figure S7c,d, Supporting Information). We speculate that disordered FeS should be the main product, although Li_2FeS_2 product displays relatively better crystallinity. Li_2FeS_2 can be seen as the combination of FeS and Li_2S. It consumes a fraction of Li_2S and leads to a residual of unbonded Fe nanodomains as shown in Figure S7d (Supporting Information). Scanning transmission electron microscope (STEM, Figure 2g) is used to further analyze the element distribution mapping of discharged FeS_2 sample. The salt and solvent components (e.g., Mg and O) are found to be present not only at the active material region (Fe and S) but also at the gel-like region, indicating a potential formation of electrolyte decomposition products, which may cover active species so as to suppress S loss from cathode. The incomplete reaction under a lower Li-salt concentration is also confirmed from the residual XRD peaks of pyrite FeS_2 as well as undecomposed TEM region with lattice fringes and diffraction spots corresponding to pyrite phase after 1st cycle (Figure S8, Supporting Information).

More solid evidences about the conversion mechanism were acquired by X-ray photoemission spectroscopy (XPS) as shown in **Figure 3**. The S2p ($S2p_{3/2}$ and $S2p_{1/2}$) spectra of pristine FeS_2 consist of two sets of peaks respectively corresponding to Fe–S (161.7 eV for $S2p_{3/2}$) and S–S (163 eV for $S2p_{3/2}$) bondings,[24,25] which are almost negligible after full discharge. Instead, at that time the peaks of Li_2S (162.1 eV for $S2p_{3/2}$) appear,[26] indicating a dominant Li-driven conversion process. When recharge to 1.7 V, the signals of Fe–S and S–S become intensified again along with remarkable weakening of those of Li_2S. The regeneration of Fe–S and S–S agrees with the formation of m-FeS_2 as shown by TEM. However in contrast to pristine sample, the intensity of S–S peaks is lower than that of Fe–S due to incomplete recovering of S–S

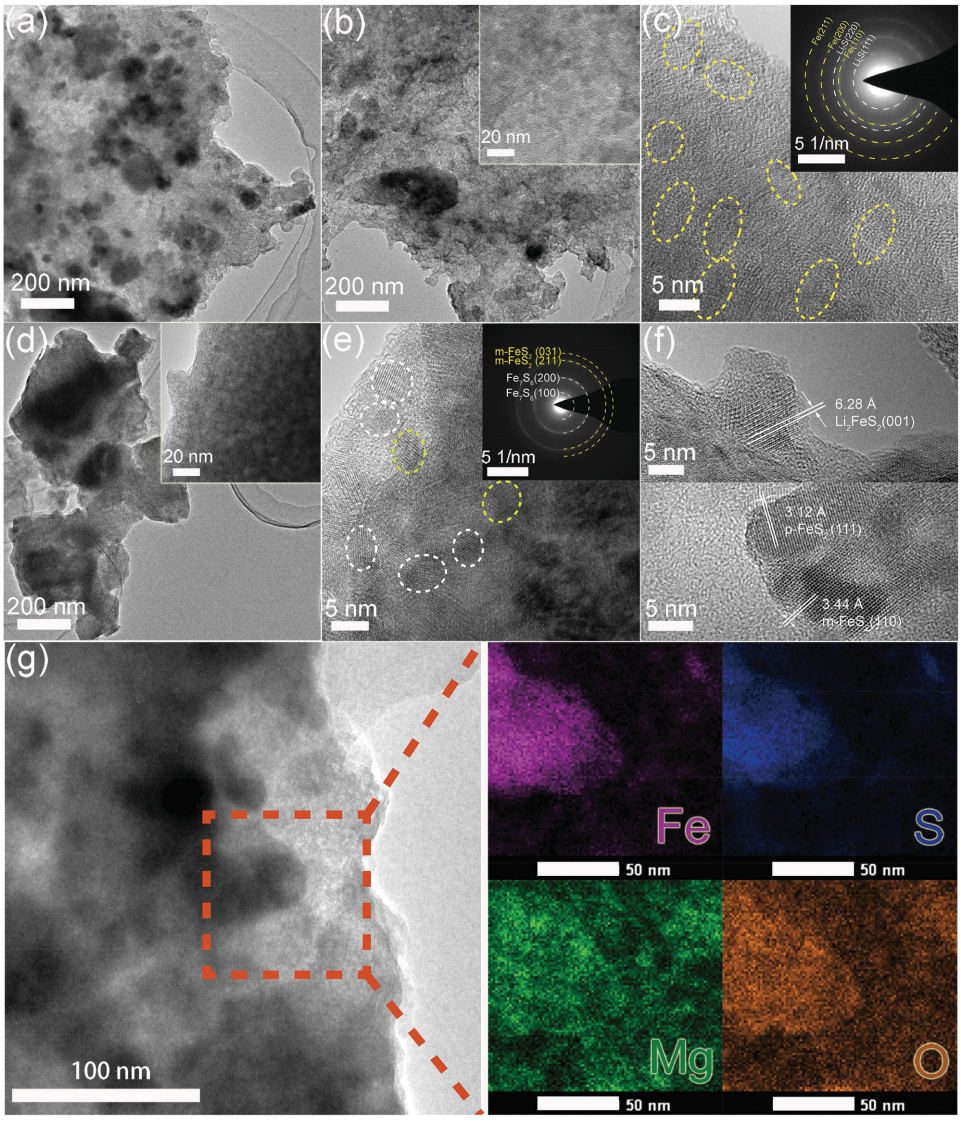

Figure 2. TEM images of FeS_2 electrodes a) after the first discharge to 0.1 V, b,c) after the second discharge to 0.1 V with different scales, d–f) after the first charge to 1.7 V with different scales and regions. Insets of (b,d): amplified TEM regions of corresponding reaction stages. Insets of (c,e): corresponding SAED patterns. g) STEM mapping of a discharged FeS_2 sample. Electrochemical amorphization and pulverization lead to a scenario that crystallized nanodomains are uniformly embedded in poorly crystallized matrix, which is still retained during the recharge process. Discharged products of Li_2S and Fe are electrochemically oxidized to m-FeS_2 and Fe_7S_8 rather than original p-FeS_2. Element mapping indicates a potential formation of electrolyte decomposition products (containing Mg and O) on active species.

bonding with the formation of S-deficient Fe_7S_8 and Li_2FeS_2. The overall intensity of XPS peaks becomes weaker after discharge and restrengthens after recharge, denoting SEI formation during lithiation and then thinning during delithiation at cathode. This SEI contains electrolyte components as indicated by detectable Mg 1s signal (Figure 3b). Its dominant peaks after discharge and recharge respectively correspond to $Mg(BH_4)_2$ at 1304.8 eV and MgH_2 at 1305.4 eV,[20,27] indicating an electrochemical dehydrogenation when electrode goes to more oxidative potentials. This dehydrogenation conversion was also verified by thermal decomposition of $Mg(BH_4)_2$ in vacuum.[28] In pristine FeS, the S2p peaks assigned to Fe–S are dominant (Figure 3c), although S-rich species is still observed near sample surface. The reversible conversion between FeS and Li_2S during cycling is verified from the discharged/charged S2p spectra. The peak intensity and Mg 1s assignment show similar changes as in the case of FeS_2 (also see Figure S9 in the Supporting Information).

3. Discussion

From the above electrochemistry and characterization, the conversion reaction of FeS_2 is mainly driven by Li rather than Mg. Since Li is not involved in either solid electrode, the reactive Li comes from the Li-ion reservoir of electrolyte and is bonded with lattice S to form Li_2S precipitate during discharge according to $FeS_2 + 4Li^+ + 4e^- \rightarrow Fe^0 + 2Li_2S$ (**Figure 4**a). At the same

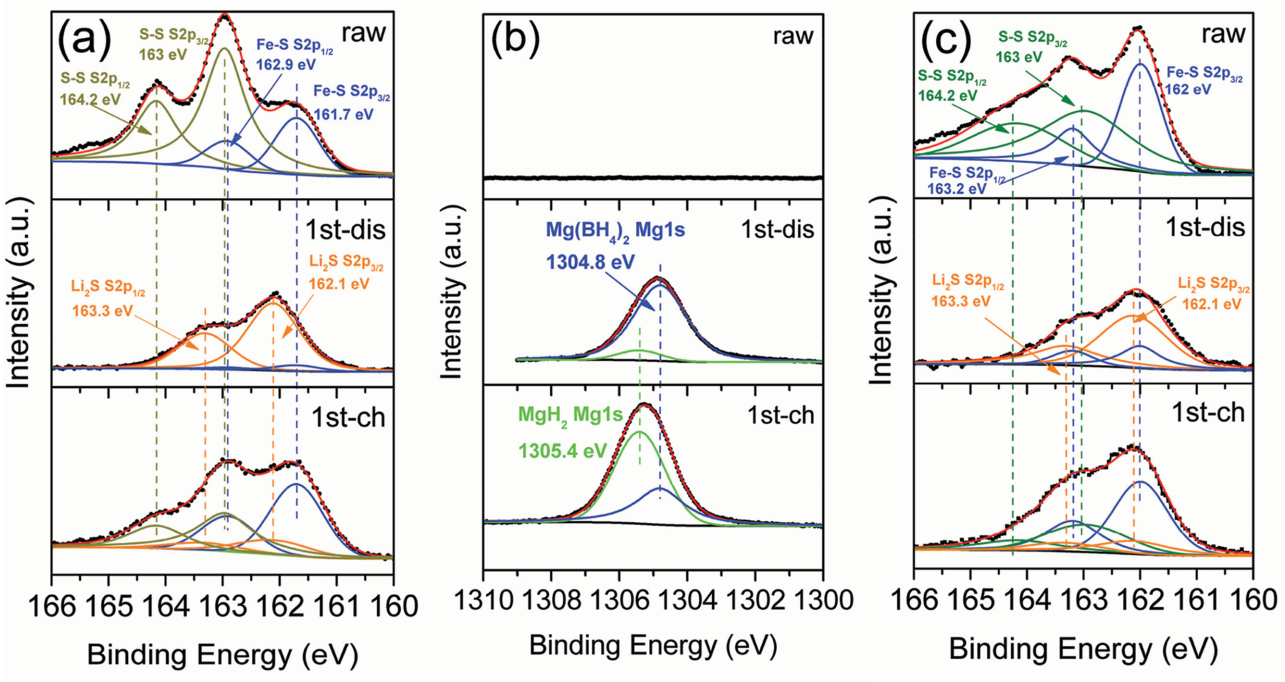

Figure 3. XPS spectra of a) S 2p and b) Mg 1s for raw, 1st discharged and 1st charged FeS_2 samples, c) S 2p for raw, 1st discharged and 1st charged FeS samples. During discharge, both the Fe–S and S–S bondings in the original sulfides are disrupted with a following formation of Li–S bonding in the Li_2S product. This process is reversible with the reappearance of Fe–S and S–S during recharging, although the exact recharged phases are different from the original phases as shown in TEM. The overall intensity change of XPS peaks indicates the formation of SEI and its thickness or component evolution. It is also implied from the detectable Mg 1s signal but with different positions of main peaks at respective discharge and recharge stages.

time, Mg^{2+} is stripped into electrolyte from metallic Mg anode ($Mg \rightarrow Mg^{2+} + 2e^-$). In the reverse process (charge to 1.7 V), the decomposed products of Li_2S and Fe nanodomains are successively oxidated to Li_2FeS_2 ($2Li_2S + Fe \rightarrow Li_2FeS_2 + 2Li^+ + 2e^-$) and m-$FeS_2$ ($Li_2FeS_2 \rightarrow Li_{2-x}FeS_2 + xLi^+ + xe^-$, $Li_{2-x}FeS_2 \rightarrow 0.8$ m-$FeS_2 + 0.2FeS_{8/7} + 0.175S + (2-x)Li^+ + (2-x)e^-$) still with poor crystallinity rather than to original p-FeS_2 phase.[13–15] Meantime Mg^{2+} is reversibly and preferentially plated back to Mg anode ($Mg^{2+} + 2e^- \rightarrow Mg$) in view of a higher standard reduction potential of Mg^{2+} than Li^+.[1] The codeposition of Mg and Li to form Mg-rich Mg-Li alloy cannot be ruled out.[29] The reversibility of m-FeS_2, Fe_7S_8, and S products with different concentration of S–S is responsible for the separate capacity regions (respectively around 1 and 0.7 V) during the following

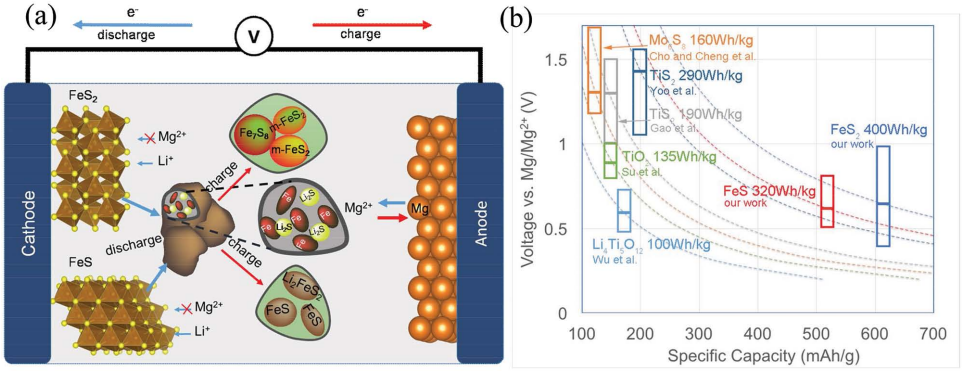

Figure 4. a) Scheme of a Li-driven conversion reaction at the FeS_x cathode coupled with polyvalent metal plating/stripping at the Mg anode. During discharge, Li^+ instead of Mg^{2+} drives the FeS_x decomposition into Li_2S and Fe nanodomains at the cathode; in the meantime Mg^{2+} is stripped from the Mg anode into the electrolyte. Since Li is not involved in either of the solid electrodes, the reactive Li comes from the Li-ion reservoir of the electrolyte. During recharge, delithiation at the cathode leads to the generation of m-FeS_2 and Fe_7S_8 products for FeS_2 and FeS and Li_2FeS_2 for FeS still with poor crystallinity similar to their discharged states. At that time, Mg^{2+} is preferentially electrodeposited back onto the Mg anode over Li^+. b) Scheme of comparison of the voltage–capacity relationship of our Mg/FeS_x systems with previous reports on Mo_6S_8,[5,6] TiS_2,[7,8] TiO_2,[9] and $Li_4Ti_5O_{12}$[10] based on the similar Mg/Li hybrid battery principle. The same energy density values are presented from dotted lines. The combination of FeS_x and Mg leads to a much higher energy density, close to 400 or 320 Wh kg^{-1}, than that of typical insertion-type sulfides and oxides (≤290 Wh kg^{-1}).

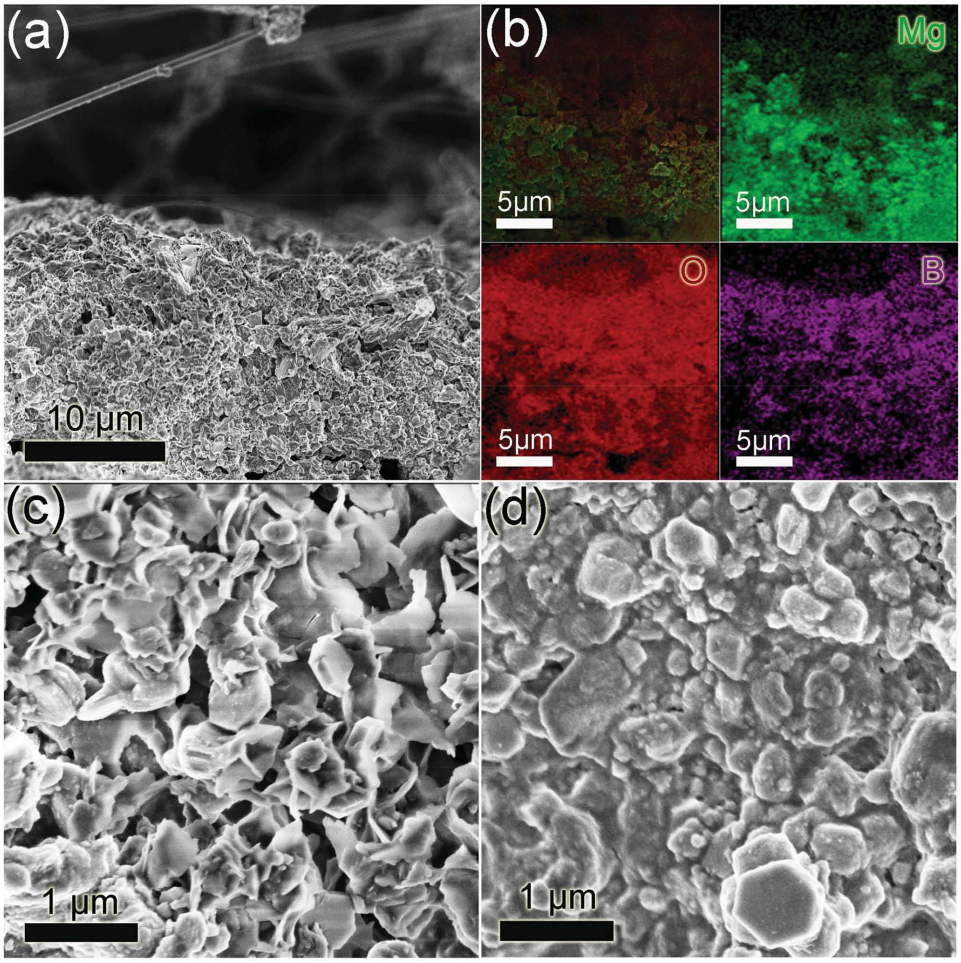

Figure 5. a) Cross-section SEM image of Mg anode of Mg/FeS_2 battery using borohydride-based electrolyte after 200 cycles. b) STEM element mapping of the corresponding region. Magnified c) cross-section and d) surface SEM images of the corresponding Mg anode. The Mg anode displays a typical morphology full of quasi-hexagonal sheets with sufficient porosity from cross-section and a more compact surface due to electrolyte components residual on grains and at grain boundaries as confirmed by element mapping. This residual likely acts as SEI to avoid quick passivation of Mg as well as S shuttle into the anode deep. The dendrite-free feature of the Mg anode is also responsible for the excellent cycling performance.

discharge (Figure 1a). In the case of FeS, the Li-driven conversion induces similar microstructure evolution and however is more reversible ($FeS + Mg + 2Li^+ \rightleftarrows Li_2S + Fe + Mg^{2+}$) since no excess Li_2S requires to be oxidated to S-rich species, which possibly dissolve during cycling. Therefore, it is understandable that electrochemical capacity greatly depends on Li-salt concentration, unless an Mg–Li alloy anode is employed to supply Li-resource from anode.[30] Although Mg-ion dissociation is activated by increasing Li-salt concentration,[20,23] its polyvalency and high polarity still limit its competition with Li ion in terms of diffusivity into host vacancies or drive force to make host structure collapse.

From the thermodynamic analysis,[31] assuming that only Mg drives the conversion reaction of FeS_2 as expressed by $FeS_2 + 2Mg \rightarrow Fe^0 + 2MgS$, the thermodynamic equilibrium voltage E_{MMB} is 1.34 V. This value is higher than that for Li-driven conversion (E_{MLB} = 1.22 V; see the Supporting Information for calculation details) according to $FeS_2 + 2Mg + 4Li^+ \rightarrow Fe^0 + 2Li_2S + 2Mg^{2+}$ in this work. This indicates that although Mg-driven conversion is thermodynamically more favorable than Li-driven one, the actual reaction progress is controlled by kinetics, i.e., solid-state diffusion rate of Mg^{2+} fall far behind compared with Li^+. Therefore, the Mg-driven reaction is at most limited at the surface of active materials. Note that the practical discharge voltage (≈0.65 V) of Mg/FeS_2 is 0.57 V smaller than E_{MLB} (Figure S10, Supporting Information). If displacing Mg anode by Li with the same borohydride-based electrolyte and salt concentration, the actual discharge voltage (≈1.5 V) of Li/FeS_2 is 0.34 V smaller than its corresponding thermodynamic equilibrium voltage E_{LMB} (1.84 V) based on $FeS_2 + 4Li \rightarrow Fe^0 + 2Li_2S$. The larger voltage deviation from thermodynamic value for Mg/FeS_2 than for Li/FeS_2 is likely caused by a stronger interaction of solvent with more charged Mg^{2+} than with Li^+, which may enhance the redox potential of $Mg(solvent)_n^{2+}/Mg$ at anode.[32]

It should be found from previous reports that most of the structure prototypes including open frameworks are not suitable for Mg-ion insertion, which is often accompanied by serious cation trapping or structure degradation.[3,33] Therefore,

circumventing slow Mg (de)bonding with structure moiety at cathode is a potential solution to high-performance Mg-based batteries. Li-driven multielectron conversion is a good candidate to achieve high energy density. Sulfides or sulfur composites have better conversion kinetics than fluoride without serious tradeoff of reaction voltage. However, rich S-bonding chemistry leads to the development of multifaceted strategies to utilize S-based anionic redox capacity and suppress S-based species dissolution. We also attempted other S-based composites, e.g., typically pyrolyzed polyacrylonitrile sulfur (PAN/S) and ordered mesoporous carbon sulfur (CMK-3/S) in the same borohydride-based electrolyte, but their performances are poor (Figure S11, Supporting Information). It seems that stricter spatial confinement of S–S bonding (e.g., S–S in FeS_2 lattice in this work) is favorable for polysulfide reversibility during cycling, compared with other spatial distributions of S–S, e.g., in small molecule (S_x, $x \leq 8$) for the case of PAN/S as well as in nanostructured S_8 for CMK-3/S.[34,35] The much better reversibility of Mg/FeS_2 also benefits from dendrite-free electroplating of Mg even after hundreds of cycles as shown in SEM of **Figure 5**. The cross-section of Mg anode shows the morphology full of quasi-hexagonal sheets with sufficient porosity. The anode surface becomes more compact due to electrolyte component residual on grains and at grain boundaries near surface, which is further confirmed by STEM mapping. This residual is expected to act as SEI to avoid quick passivation of Mg as well as S shuttle into the anode deep (negligible S signal at anode from STEM mapping even after 200 cycles). In chloride-based electrolyte system, the rougher anode surface with thicker Mg precipitates observed merely after 15 cycles may be partially responsible for the worse electrochemistry (Figure S12, Supporting Information). The morphology discrepancy of Mg surfaces is associated with the degree of polysulfide dissolution, Mg plating/stripping efficiency and overpotential in respective electrolyte as well as passivation situation on anode, which would alter the nucleation and growth modes of Mg.[20,36]

4. Conclusion

In summary, we have proposed a Mg-based battery characterized by high capacity conversion reaction at cathode. This system combines the advantages of kinetically favorable Li-driven conversion of FeS_x and smooth Mg plating/stripping by using a dual-salt Mg^{2+}/Li^+ electrolyte. It simultaneously bypasses sluggish Mg-ion diffusion in host lattice at the cathode as well as lithium dendrite propagation at the anode. At the anode side, smoother Mg plating (no dendrites after hundreds of cycles) brings about more stable cycling than sharper Li electrodeposition. SEI-containing electrolyte components are in situ formed at both the cathode and the anode, and are favorable to suppress polysulfide dissolution from the cathode, S shuttle to bulk Mg, and quick anode passivation. The combination of FeS_2 and Mg render this hybrid battery a much higher energy density close to 400 Wh kg^{-1} compared with similar systems with insertion-type sulfides and oxides (≤290 Wh kg^{-1}, Figure 4b).[5–10] This energy density is competitive to that of LIBs based on $LiCoO_2$ or $LiFePO_4$. This work paves the way to explore advanced multielectron (hybrid) systems coupled with safe Mg anodes (e.g., Mg–S batteries). Their energy densities would hopefully be further improved by carefully choosing combinations of cathode and electrolyte.

Supporting Information

Supporting Information is available from the Wiley Online Library or from the author.

Acknowledgements

This work was supported by the National Natural Science Foundation of China under Grant No. 51372263 and by the Key Research Program of Chinese Academy of Sciences under Grant No. KGZD-EW-T06. C.L.L. would like to thank the supports from the "Hundred Talents" program of the Chinese Academy of Sciences and the Science Foundation for Young Researchers of State Key Laboratory of High Performance Ceramics and Superfine Microstructures. The authors thank Z. H. Cui, X. X. Guo, and J. L. Wang for their experimental helps.

Received: August 27, 2015
Revised: September 21, 2015
Published online: November 5, 2015

[1] J. Muldoon, C. B. Bucur, T. Gregory, *Chem. Rev.* **2014**, *114*, 11683.
[2] D. Aurbach, Z. Lu, A. Schechter, Y. Gofer, H. Gizbar, R. Turgeman, Y. Cohen, M. Moshkovich, E. Levi, *Nature* **2000**, *407*, 724.
[3] E. Levi, M. D. Levi, O. Chasid, D. Aurbach, *J. Electroceram.* **2009**, *22*, 13.
[4] S. Yagi, T. Ichitsubo, Y. Shirai, S. Yanai, T. Doi, K. Murase, E. Matsubara, *J. Mater. Chem. A* **2014**, *2*, 1144.
[5] Y. W. Cheng, Y. Y. Shao, J. G. Zhang, V. L. Sprenkle, J. Liu, G. S. Li, *Chem. Commun.* **2014**, *50*, 9644.
[6] J. H. Cho, M. Aykol, S. Kim, J. H. Ha, C. Wolverton, K. Y. Chung, K. B. Kim, B. W. Cho, *J. Am. Chem. Soc.* **2014**, *136*, 16116.
[7] T. Gao, F. D. Han, Y. J. Zhu, L. M. Suo, C. Luo, K. Xu, C. S. Wang, *Adv. Energy Mater.* **2015**, DOI: 10.1002/aenm.201401507.
[8] H. D. Yoo, Y. L. Liang, Y. F. Li, Y. Yao, *ACS Appl. Mater. Interfaces* **2015**, *7*, 7001.
[9] a) S. J. Su, Z. G. Huang, Y. N. NuLi, F. Tuerxun, J. Yang, J. L. Wang, *Chem. Commun.* **2015**, *51*, 2641; b) F. Tuerxun, Y. Abulizi, Y. N. NuLi, S. J. Su, J. Yang, J. L. Wang, *J. Power Sources* **2015**, *276*, 255.
[10] a) N. Wu, Z. Z. Yang, H. R. Yao, Y. X. Yin, L. Gu, Y. G. Guo, *Angew. Chem. Int. Ed.* **2015**, *127*, 5849; b) N. Wu, Y. C. Lyu, R. J. Xiao, X. Q. Yu, Y. X. Yin, X. Q. Yang, H. Li, L. Gu, Y. G. Guo, *NPG Asia Mater.* **2014**, *6*, 120.
[11] S. S. Zhang, *J. Mater. Chem. A* **2015**, *3*, 7689.
[12] J. Liu, Y. R. Wen, Y. Wang, P. A. van Aken, J. Maier, Y. Yu, *Adv. Mater.* **2014**, *26*, 6025.
[13] S. B. Son, T. A. Yersak, D. M. Piper, S. C. Kim, C. S. Kang, J. S. Cho, S. S. Suh, Y. U. Kim, K. H. Oh, S. H. Lee, *Adv. Energy Mater.* **2014**, *4*, 1300961.
[14] T. Evans, D. M. Piper, S. C. Kim, S. S. Han, V. Bhat, K. H. Oh, S. H. Lee, *Adv. Mater.* **2014**, *26*, 7386.
[15] T. A. Yersak, H. A. Macpherson, S. C. Kim, V. D. Le, C. S. Kang, S. B. Son, Y. H. Kim, J. E. Trevey, K. H. Oh, C. Stoldt, S. H. Lee, *Adv. Energy Mater.* **2013**, *3*, 120.
[16] C. B. Zhu, Y. R. Wen, P. A. van Aken, J. Maier, Y. Yu, *Adv. Funct. Mater.* **2015**, *25*, 2335.
[17] D. Aurbach, E. Pollak, R. Elazari, G. Salitra, C. S. Kelley, J. Affinito, *J. Electrochem. Soc.* **2009**, *156*, A694.

[18] C. Huang, J. Xiao, Y. Y. Shao, J. M. Zheng, W. D. Bennett, D. P. Lu, S. V. Laxmikant, M. Engelhard, L. W. Ji, J. G. Zhang, X. L. Li, G. L. Graff, J. Liu, *Nat. Commun.* **2014**, *5*, 3015.
[19] R. G. Cao, W. Xu, D. P. Lv, J. Xiao, J. G. Zhang, *Adv. Energy Mater.* **2015**, DOI: 10.1002/aenm.201402273.
[20] Y. Y. Shao, T. B. Liu, G. S. Li, M. Gu, Z. M. Nie, M. Engelhard, J. Xiao, D. P. Lv, C. M. Wang, J. G. Zhang, J. Liu, *Sci. Rep.* **2013**, *3*, 3130.
[21] Y. S. Su, Y. Z. Fu, T. Cochell, A. Manthiram, *Nat. Commun.* **2013**, *4*, 2985.
[22] H. S. Kim, T. S. Arthur, G. D. Allred, J. Zajicek, J. G. Newman, A. E. Rodnyansky, A. G. Oliver, W. C. Boggess, J. Muldoon, *Nat. Commun.* **2011**, *2*, 427.
[23] a) R. Mohtadi, M. Matsui, T. S. Arthur, S. J. Hwang, *Angew. Chem. Int. Ed.* **2012**, *51*, 9780; b) O. Tutusaus, R. Mohtadi, *ChemElectroChem* **2015**, *2*, 51; c) R. Mohtadi, F. Mizuno, *Beilstein J. Nanotechnol.* **2014**, *5*, 1291.
[24] H. W. Nesbitt, G. M. Bancroft, A. R. Pratt, M. J. Scaini, *Am. Mineral.* **1998**, *83*, 1067.
[25] G. Panzner, B. Egert, *Surf. Sci.* **1984**, *144*, 651.
[26] K. M. Abraham, S. M. Chaudhri, *J. Electrochem. Soc.* **1986**, *133*, 1307.
[27] K. Tajima, Y. Yamada, S. H. Bao, M. Okada, K. Yoshimura, *Sol. State Ion.* **2009**, *180*, 654.
[28] M. Chong, A. Karkamkar, T. Autrey, S. Orimo, S. Jalisatgi, C. M. Jensen, *Chem. Commun.* **2011**, *47*, 1330.
[29] J. Chang, R. T. Haasch, J. Kim, T. Spila, P. V. Braun, A. A. Gewirth, R. G. Nuzzo, *ACS Appl. Mater. Interfaces* **2015**, *7*, 2494.
[30] T. Ichitsubo, S. Okamoto, T. Kawaguchi, Y. Kumagai, F. Oba, S. Yagi, N. Goto, T. Doid, E. Matsubara, *J. Mater. Chem. A* **2015**, *3*, 10188.
[31] C. X. Zu, H. Li, *Energy Environ. Sci.* **2011**, *4*, 2614.
[32] T. Ichitsubo, S. Yagi, R. Nakamura, Y. Ichikawa, S. Okamoto, K. Sugimura, T. Kawaguchi, A. Kitada, M. Oishi, T. Doi, E. Matsubara, *J. Mater. Chem. A* **2014**, *2*, 14858.
[33] R. G. Zhang, X. Q. Yu, K. W. Nam, C. Ling, T. S. Arthur, W. Song, A. M. Knapp, S. N. Ehrlich, X. Q. Yang, M. Matsui, *Electrochem. Commun.* **2012**, *23*, 110.
[34] J. L. Wang, Y. S. He, J. Yang, *Adv. Mater.* **2015**, *27*, 569.
[35] X. L. Ji, K. T. Lee, L. F. Nazar, *Nat. Mater.* **2009**, *8*, 500.
[36] N. Pour, Y. Gofer, D. T. Major, D. Aurbach, *J. Am. Chem. Soc.* **2011**, *133*, 6270.